Available online at www.sciencedirect.com
SCIENCE DIRECT®
Journal of Catalysis 221 (2004) 137–147
JOURNAL OF CATALYSIS
www.elsevier.com/locate/jcat

SCR of lean NO_x with C_3H_8 over Co/MFI catalysts: dependence on synthesis condition of MFI and Co location

X.-Y. Chen,[1] S.-C. Shen, H.-H. Chen, and S. Kawi *

Department of Chemical & Environmental Engineering, National University of Singapore, 10 Kent Ridge Crescent, Singapore 119260, Republic of Singapore

Received 6 May 2003; revised 25 July 2003; accepted 28 July 2003

Abstract

The effects of different synthesis conditions for MFI and the different locations of Co^{2+} on MFI on the catalyst properties for the selective catalytic reduction of NO by C_3H_8 [C_3H_8–SCR] in the presence of excess oxygen were investigated, and the nature of Co^{2+} was characterized by XRD, FTIR, H_2-TPR, XPS, and DTG. H_2-TPR shows that the exchanged Co ions in MFI are nonreducible even at 750 °C, while the reduction temperature of incorporated Co is at 690 °C. Three types of DTG peaks, which correspond to different temperatures for the thermal decomposition or disassociation of TPA, are observed in the differential thermogravimetric (DTG) analysis of the as-synthesized MFI prepared under different conditions, and are related well to C_3H_8–SCR of NO for three different types of Co sites in MFI: incorporated Co^{2+} site and two different exchanged Co^{2+} sites, respectively. The incorporated Co^{2+} in MFI with the DTG peak temperature at 418 °C is almost inactive for C_3H_8–SCR of NO. For the Co^{2+}-exchanged MFI, the sample with a low Co^{2+}-exchange degree has a higher TOF for NO reduction than that having a higher Co^{2+}-exchange degree, indicating that at least two types of Co^{2+} sites exist in the Co^{2+}-exchanged MFI sample. The corresponding DTG peak temperatures located at 455 and 481 °C show two types of exchanged Co ion sites having different surface energies for different activities for SCR of NO, with the Co^{2+} site with higher surface energy having higher specific catalytic activity for NO reduction. The exchange degree and position of Co^{2+} depend on the alkalinity of the hydrothermal synthesis condition and the sodium content of the resulting Co^{2+}-exchanged MFI.

Keywords: SCR; NO_x; MFI; Cobalt ion exchange; Cation location; Incorporation; DTG

1. Introduction

NO emission into the atmosphere is a worldwide concern because it contributes to acid rain, urban smog, and ozone exhaust. There are a number of approaches to NO removal under oxygen-rich conditions aimed for stationary and lean-burn engine sources. Among them, selective catalytic reduction by hydrocarbons [HC–SCR] is believed to be a potential technology for removal of NO from exhaust since it was reported in 1990 [1,2]. One family of catalysts that show promising performance with CH_4 and other hydrocarbons is cobalt-containing MFI, which have been extensively investigated recently by many research groups [3–35]. There are many advantages for Co/MFI catalysts. For example, Co ion-exchanged MFI catalysts are more effective than Cu- or Fe-MFI under rich-oxygen conditions [3,4,19] and show unusual hydrothermal stability [5,6,36,37]. Its catalytic performance for HC–SCR of NO was even improved by hydrothermal treatment [38]. Furthermore, as compared to Pt-containing catalysts, which reduce NO mainly to N_2O [39,40], Co/MFI does not produce N_2O during HC–SCR of NO [3,8] and even shows activity for decomposition of N_2O [41,42].

However, for HC–SCR of NO over Co/MFI, there are still a lot of controversial results in the literature on the role of oxygen [3,4,15,21,23,24,29,43] and active species [4,8–10,21,27,30,34] and the influence of cobalt content [4, 20,28–30,43] on the activity of the catalysts. Some authors pointed that the high activity of cobalt incorporated ZSM-5 for NO_x reduction was due to the incorporation of Co^{2+} in the siliceous MFI structure [9,34]. It is also generally accepted, however, that NO conversion increases with Co ions in MFI within the range of exchange capacity [4,20,28].

* Corresponding author.
E-mail address: chekawis@nus.edu.sg (S. Kawi).
[1] Present address: Department of Chemical Engineering, University of Michigan, Ann Arbor, MI 48109.

0021-9517/$ – see front matter
doi:10.1016/j.jcat.2003.07.008

With a further increase of exchange degree, the activity for HC–SCR of NO is not linearly proportional to the loading of Co ions in MFI [4,20,29,43]. These results suggest that there exist different Co ions having different activities in MFI [30,43,44]. In other words, there may exist different cation positions within the channels of MFI. Actually for Co ions, at least two different kinds of sites and coordination to framework and oxygen have been found [45–47]. For CH_4–SCR of NO, it has been found that the alpha-type Co^{2+} ions, which are located in the main channel of mordenite and ferrierite and coordinated above the rectangle of four framework oxygen of the channel wall, exhibit the highest activity in these zeolites; however, the beta-type Co^{2+} ions coordinated in the plane of four oxygen of the deformed six-member ring located in the channel intersection of ZSM-5 and in channels of beta zeolite control the activity of these Co zeolites [48]. Therefore, the preparation conditions, such as loading method of cobalt species, play a strong role in the catalyst activity for HC–SCR of NO [15,16,22]. It is well known that the catalytic activity of zeolite materials often depends on the structural properties of zeolite, which in return is controlled by hydrothermal conditions used during synthesis. Up to now, the studies reported in literature for the improvement of HC–SCR of NO over Co/MFI were focused on the modification of different loading conditions and methods of cobalt species by post-treatment in MFI [15, 22,28,29,49]. Very little attention has focused on the effect of hydrothermal synthesis conditions of MFI for HC–SCR of NO. This paper reports that the pH used in the starting synthesis gel has a great influence on the ion-exchange capacity and the distribution of different exchangeable cation positions in synthesized MFI. The later controls the loading of Co ions in MFI channels and therefore controls the activity of Co/MFI catalysts for C_3H_8–SCR of NO. To further study the nature of active Co ions for HC–SCR of NO, the present work also compares the catalytic activities and properties of Co-incorporated and Co-exchanged MFI catalysts.

2. Experimental

2.1. MFI synthesis and catalyst preparation

Na-MFI materials having a Si/Al mole ratio of 15 in the starting gel [denoted here as Z] were synthesized using tetrapropylammonium hydroxide [TPAOH] as a structurally directing agent according to synthesis procedures described in the literature [50]. The composition of reaction gel was SiO_2:0.033 Al_2O_3:0.1 Na_2O:0.04 $[TPA]_2O$:35 H_2O. In a typical synthesis, solution A was obtained by adding 60 g of Ludox HS-40 [40 wt%, Aldrich] into 34 g of water under stirring. Then under stirring, 2.13 g of NaOH and 2.19 g of $NaAlO_2$ were added to a mixture of 32.5 g of 20% TPAOH [Merck] and 150 g of water to form solution B. After stirring for 30 min, solution A was added dropwise into solution B. The pH in the reaction gel mixture was adjusted by H_2SO_4. After stirring the resulting mixture for another 90 min, the reaction gel was transferred into Teflon-lined autoclaves and then heated statically at 170 °C for 72 h. The solid products were recovered by filtration, washed with deionized water, and then dried at 100 °C. Finally the as-synthesized samples were calcined in air at 560 °C for 15 h.

Co^{2+}-exchanged MFI, denoted here as Co-Z, was prepared from the calcined Na-MFI by the conventional solution cation-exchange method using 0.1 N of cobalt nitrate solution and solid to solution ratio of 1:20. In order to make sure that the reaction in the NO–C_3H_8–O_2 system is kinetically controlled by surface reaction over Co/MFI, a low cation-exchange degree [CED] of Co ions in MFI is required, yielding Co species as Co^{2+} after dehydration. Therefore, the ion-exchange process was performed at room temperature. Typically 2 g of solid sample was added into 40 ml of 0.1 N $Co(NO_3)_2$ aqueous solution and the mixture was stirred at room temperature for 24 h. The solid product was recovered and washed by centrifugation. After repeating this ion exchange process for 3 times, the solid products were dried at 100 °C overnight and then calcined in air at 600 °C for 6 h. The CED of Co^{2+} was calculated from ICP analysis results based on the assumption that one Co^{2+} ion replaces two Na^+ ions required for balancing two framework aluminum atoms. For example, a Co/Al ratio of 0.5 provides 100% CED of Co^{2+}.

Co^{2+} incorporated MFI having a Si/Al mole ratio of 20, which is denoted here as Z05, was directly synthesized by adding $CoCl_2$ solution into the above-stated gel mixture without the addition of sodium aluminate. The synthesis followed the general procedure described in the literature [51]. Typically 2.13 g of NaOH and 60 g of Ludox HS-40 were added into 164 g of water under stirring. After stirring for 30 min, H_2SO_4 was added dropwise to adjust the pH down to 12 before 32.5 g of 20% TPAOH was added to the mixture. After stirring the mixture for another 30 min, 20 ml of aqueous solution containing 4.76 g of $CoCl_2 \cdot 6H_2O$ was added into the above gel. The following-up procedures for crystallization, washing, and drying were the same as those used in Na-MFI synthesis.

2.2. Catalyst characterization

X-ray diffraction [XRD] analysis was carried out using a Shimadzu XRD-6000 X-ray diffractometer with Cu-K_α radiation. The voltage and current applied were 40 kV and 30 mA, respectively. The step size and count time were 0.02° and 0.3 s, respectively. The slit values used were 1.0 [DS], 1.0 [SS], and 0.30 [RS]. The crystallinity of the sample was calculated from the integrated intensity based on the characteristic diffraction peaks at $2\theta = 7$–9 and 22.5–24.5°. The bulk chemical analysis of the cobalt-containing MFI after acid [HF] digestion of the solid was obtained using induced coupled plasma [ICP] atomic absorption.

The framework vibration for as-synthesized, calcined, or Co-exchanged samples was performed on a Shimadzu FTIR-8700 infrared spectrophotometer using KBr pellets. The infrared spectra characterizing the surface hydroxyl groups were recorded after treatment of the self-supported sample wafer under vacuum ($< 10^{-5}$ mbar) at 150 °C for 2 h. The H-type samples required for the characterization of surface hydroxyl groups were prepared by exchanging calcined Na-MFI or sample Z05 with NH_4^+ in 1.0 N $(NH_4)NO_3$ aqueous solution at 60 °C under stirring for 10 h. After the solid was recovered and washed by filtration, it was dried at 110 °C and finally calcined at 450 °C for 4 h.

Thermogravimetric analysis of the as-synthesized sample was carried out on a TGA 2050 Thermogravimetric Analyzer (TA Instrument) with a N_2 flow of 100 ml/min and a heating rate of 10 °C/min.

Specific surface areas of samples were determined by the N_2 BET method at liquid nitrogen temperature using Quantachrome Autosorb-1.

Temperature-programmed reduction [TPR] experiments were carried out in a flow tubular quartz reactor loaded with 50 mg of catalyst. A thermocouple placed in the upper side of the sample bed was used to monitor the catalyst temperature. The reducing gas mixture was composed of 5% of H_2 and 95% of N_2. A column of 3A zeolite placed in GC was used to remove the water formed during TPR experiment. The H_2 consumption was analyzed by TCD using a current of 60 mA. Prior to the TPR experiment, the sample was pretreated in dry 25% O_2/75% He with a flow of 30 ml/min at 600 °C for 2 h.

X-ray photoelectron spectroscopy [XPS] spectra of cobalt-containing samples were obtained using a Kratos AXIS spectrometer equipped with monochromatic Al-K_α X-rays [1486.6 eV, 225 W]. The analyzer was operated at a pass energy of 80 eV. Binding energies were referenced to C1s line at 284.6 eV with an accuracy of ±0.1 eV. The measurements were performed at room temperature. The Co_{2p} as well as Al_{2p}, O1s, and Si_{2p} core levels were thoroughly determined. All spectra were fitted with a Gaussian method in order to determine the number of components under the XPS peaks.

2.3. Catalytic reactions

Selective catalytic reduction [SCR] of NO was carried out using an ordinary continuous flow-type reactor operating at ambient pressure. 0.45 g (∼0.8 ml) of catalyst was packed in a tubular reactor and the flow rates of all gases were controlled by mass flow controllers. The gas inlet into the reactor with a total flow of 200 ml/min consisted of 1000 ppm of NO, 15 or 5% of O_2, 1000 ppm of C_3H_8, and helium as the balance gas, which corresponded to a GHSV of 15,000 h^{-1}. The analysis of NO and O_2 concentrations was carried out using a Shimadzu NOA-7000 NO/O_2 chemiluminescence analyzer. The concentrations of C_3H_8, H_2O and N_2O were analyzed using a Shimadzu GC-17A with TCD as the detector. All data were collected after the reaction system has been stabilized for at least 30 min at each reaction temperature. The conversions of NO and C_3H_8 were calculated based on their compositions at the inlet and outlet of the reactor. Therefore, the TOF for NO reduction over Co/MFI was calculated based on the steady-state NO conversion and Co content in Co/MFI.

3. Results and discussion

3.1. MFI synthesis and characterization

Table 1 summarizes the gel and bulk compositions and properties of the prepared catalysts as well as the influence of crystallization temperature on the crystallinity of MFI. Under the same alkalinity [pH 13.5], the low synthesis temperature at 150 °C [Z01] yields lower MFI crystallinity as compared to those synthesized at high temperature at 170 °C [Z02]. The crystallinity of MFI also decreases with the decrease of alkalinity in the starting gel, leading to the formation of amorphous silica at pH 10.5 [as found in Z03]. However, too high alkalinity [pH ⩾ 14] also results in the low yield of MFI because most silica species are dissolved in the mother solution. When the crystallization temperature is fixed at 170 °C, a comparison of Z02 and Z04 shows that

Table 1
Synthesis conditions and properties of MFI and Co/MFI catalysts

Sample	Synthesis condition				Product properties							
	Temp. (°C)	pH	Si/Al Gel[a]	Si/Co Gel[a]	Si/Al[b]	Si/Co[b]	Na/Al[c]	Na/Co[c]	Crystallinity[c] (%)	BET (m^2/g)	Co content (wt%)[b]	Co/Al[b]
Z01	150	13.5	15	∞					82			
Z02	170	13.5	15	∞	10		0.93		100	358		
Z03	150	10.5	15	∞					Amorphous			
Z04	170	12	15	∞	13		0.57		97	369		
Z05	170	12	∞	20	560	23		0.14	88	438	4.21	
Co-Z02	Co-ions exchanged MFI										1.15	0.18
Co-Z04	Co-ions exchanged MFI										0.16	0.04

[a] Atomic ratio calculated from synthesis recipe.
[b] Results of ICP analysis.
[c] ICP analysis of as-synthesized forms.

the crystallinity of MFI is not affected by the alkalinity in the range of pH 12–13.5.

It can be seen from Table 1 that aluminum atoms are easily incorporated into the tetrahedral framework of MFI structure, and the atomic ratio of Si to Al in Z02 and Z04 is 10 and 13, respectively. The difference in the BET specific surface area between Z02 and Z04 is less than 3% for pH from 12 up to 13.5. However, the loading of exchanged Co ions in MFI depends greatly on pH. The cobalt content in Co-Z02 is 1.15 wt% (Co/Al = 0.18), which is 4.5 times more in Co-Z04 (Co/Al = 0.04) having only 0.16 wt% of Co, although Co was loaded onto the two samples under the same solution-exchange conditions. It is worth noting that the difference in pH during synthesis also influences the Na content in MFI. Na/Al atomic ratios for as-synthesized Z02 and Z04 are 0.93 and 0.57, respectively, indicating that a portion of cationic sites in MFI are occupied by other cations, probably by TPA^+, and more cationic sites in Z04 than in Z02 are not occupied by Na^+ to balance the charge.

Since Al^{3+} is known to be an amphoteric ion, it can be present as AlO_2^- in a basic solution. Furthermore, AlO_2^- can then easily coordinate with Si–O–Si tetrahedral during hydrothermal crystallization to form tetrahedral aluminosilicate. Thus high alkalinity favors the incorporation of aluminum into the MFI framework. In contrast to Al^{3+}, the strong polarization of cobalt ion leads to the precipitation of cobalt hydroxide in basic solution. Therefore, for better incorporation of cobalt species into the framework of MFI structure, the pH of the starting gel during the synthesis of Co-incorporated MFI [Z05] was selected to be the same as that of Z04. However, the Na/Co atomic ratio in Z05 is only 0.14.

Fig. 1 shows the XRD patterns of as-synthesized MFI prepared under different synthesis conditions. It can be seen that Z04 and Z02 have the same XRD patterns, although they are synthesized under different pH in gel. XRD patterns show that the inclusion of Co into the MFI framework results in the partial distortion of lattice and the orientation growth of the framework structure of MFI crystal. We compare XRD patterns of Z05 with Z04 because the synthesis pH for these two samples is the same (pH 12). The characteristic double peaks in Z04 at 2θ around 45° become one peak at 45.38° in Z05. Furthermore, the two peaks at $2\theta = 26.52$ and 26.78° in Z04 become one peak at 26.69° in Z05. Fig. 2 further shows the effects of Co ions exchanged at the cation positions or Co incorporated into Si–O–Si tetrahedral sites on the lattice structure of MFI. After Co loading, XRD patterns for both Co ion-exchanged Z02 and Z04 remain unchanged and the same as those before ion exchange. However, the transformation of original orthorhombic symmetry to monoclinic symmetry is observed in Z05, with the peak at 24.26° in Fig. 1 splitting into two peaks at 24.22 and 24.38° in Fig. 2. From the structural coordination point of view, the crystalline ionic radius of four-coordinate Si^{4+} is 0.40 Å [52], which is close to that of four-coordinate Al^{3+} [0.53 Å]. However, the crystalline ionic radius of Co^{2+} for

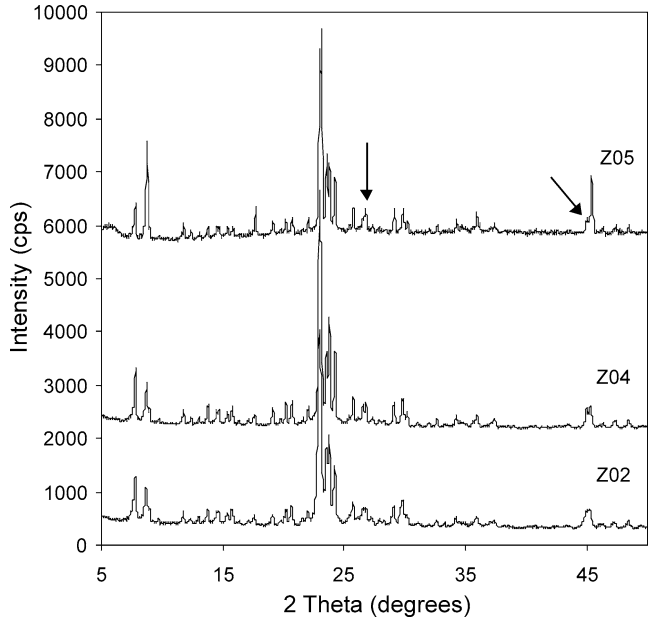

Fig. 1. XRD patterns of as-synthesized MFI obtained under different synthesis conditions.

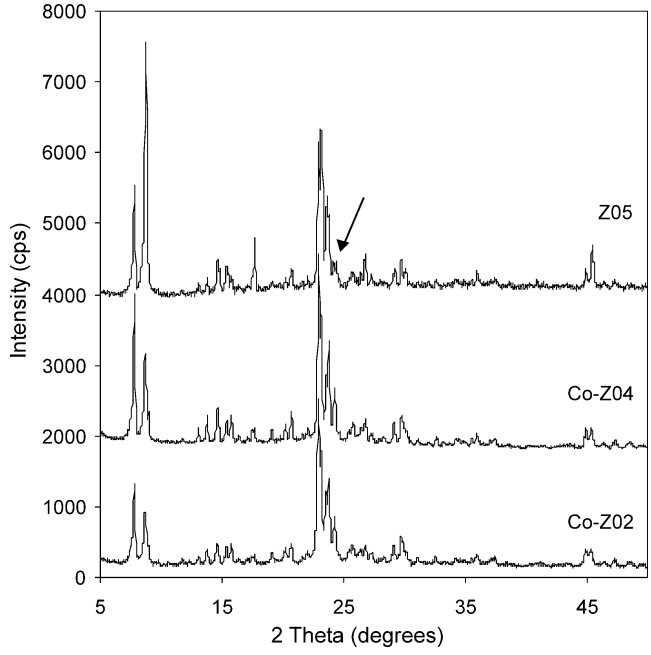

Fig. 2. XRD patterns of calcined Co-incorporated and Co-exchanged MFI samples.

IV coordination is 0.72 Å, which is appreciably larger than that of Si^{4+}. Therefore, the incorporation of Co species into the framework of MFI structure requires a substantial lattice rearrangement and results in a distorted tetrahedral lattice.

The framework vibrational IR spectra are used to distinguish the local structures after Co ions have been exchanged to the cation positions or Co incorporated into the framework of MFI. Fig. 3 shows the FT-IR spectra of different MFI. Once compared with Na-MFI (Z04), a weak band at

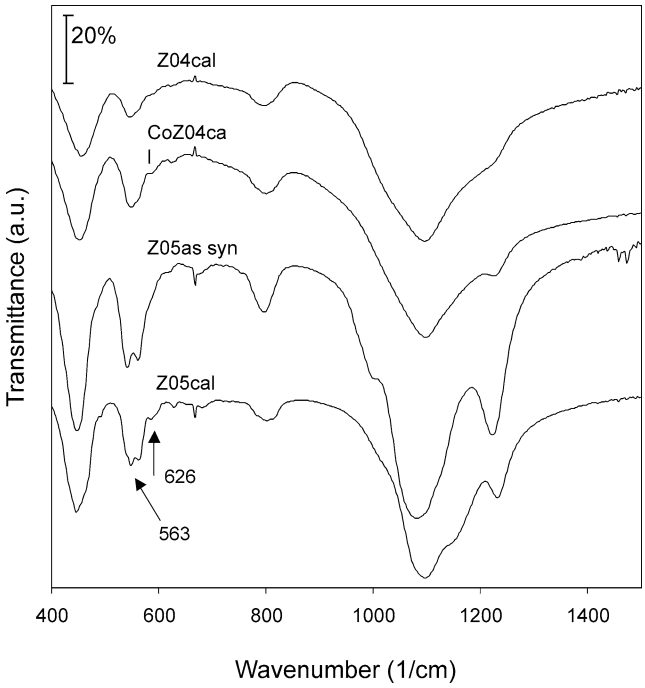

Fig. 3. FTIR spectra characterizing framework vibration of different MFI samples.

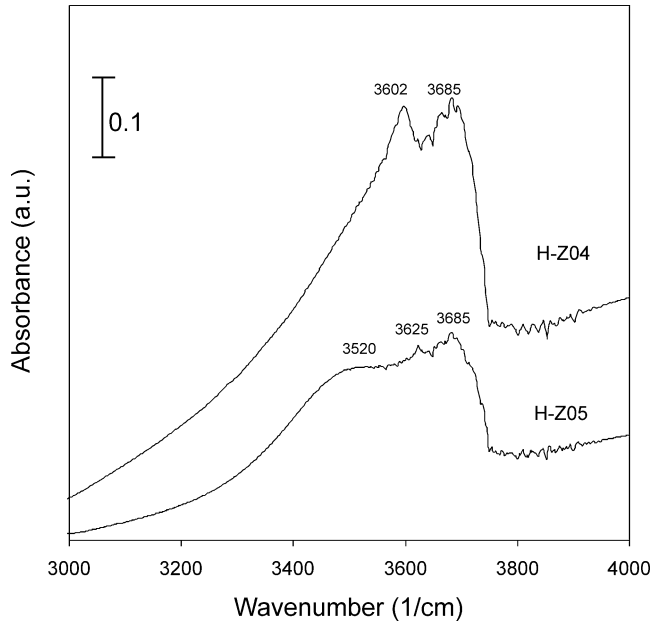

Fig. 4. FTIR spectra of hydroxyl groups on H^+-type Z04 and Z05 samples.

626 cm^{-1} is observed for Co-exchanged (Co-Z04) and incorporated (Z05) samples. According to the assignments of the infrared peak of zeolites by Flanigen et al. [53], the vibration bands located at 500–650 cm^{-1} are assigned to structurally sensitive external linkages. In this study, this vibration band is assigned to the presence of exchanged Co^{2+} ions at the cation positions of MFI. The presence of 626 cm^{-1} band in Z05 should be attributed to Co ions to balance the electrical neutrality of MFI framework due to the incorporation of cobalt into MFI framework. There always exist exchangeable Co^{2+} ions in Z05 occupying the exchangeable cation sites. The amount of the exchanged Co^{2+} ions in Z05 depends on the competition among Co^{2+}, Na^+, and probably template TPA^+ in the synthesis gel and on the amount of incorporated cobalt. A new band around 563 cm^{-1}, which is close to the structurally sensitive absorption band at 550 cm^{-1} for MFI structure [54,55], is observed only for Z05. This new band can be assigned to double ring vibration based on the band assignment reported in the literature [53–55], showing that cobalt species in Z05 have entered the five-membered rings of T sites in the MFI framework.

In order to further compare the difference between Z04 and Z05, Fig. 4 shows the IR spectra of H-MFI (H-Z04) and H-type Co-incorporated MFI (H-Z05). The hydroxyl groups on the two samples are obviously different. The absorbance (ABS) intensity of hydroxyl groups for H-Z05 is lower and its IR band is broader than that of H-Z04, showing that the surface concentration of hydroxyl groups on H-Z04 is higher than that on H-Z05. It is also noted that there exists two IR bands at 3602 and 3685 cm^{-1}, respectively, indicating that two kinds of hydroxyl groups are present on the surface of H-Z04. These two kinds of hydroxyl groups may associate with different energetic sites and coordination environment for exchangeable cations. Thus, two kinds of Co^{2+} may exist on Z04 MFI catalysts and they may have different specific catalytic activity for C_3H_8–SCR of NO.

3.2. Differential thermogravimetric analysis

The different loading of Co ions in Z02 and Z04 indicates that the pH used in the synthesis of MFI has a great influence on cation-exchanged degree, although XRD and FTIR results show that their crystalline and framework structures remain the same, and the ICP result (Table 1) shows a similar Si/Al ratio in Z02 and Z04. EPR, in situ XPS, and UV–vis diffuse reflectance spectroscopic results [45–47] showed that Co ions occupied at least two different ionic sites in MFI: the α-type Co ions located at the straight channel wall of MFI and the β-type Co ions located at the intersection of straight and sinusoidal channels. The presence of these two different Co ions and the fact that β-type Co ions have been shown to have the highest activity for CH_4–SCR of NO over Co/MFI [30] drive us to investigate the effect of different exchangeable cation positions in Z02 and Z04 on the reduction of NO by propane. Furthermore, the cobalt species present in our Co-containing MFI catalysts can be either incorporated into the framework of MFI or exchanged at the cationic sites of the extraframework of MFI. Therefore, it is important to relate the catalyst activity for SCR of NO with both incorporated and exchanged Co species in MFI.

In this study, a thermal analysis technique is used to correlate the removal of templated TPA^+ with different types of cobalt species in MFI. Fig. 5 shows the DTG curves of as-synthesized MFI prepared under different synthesis con-

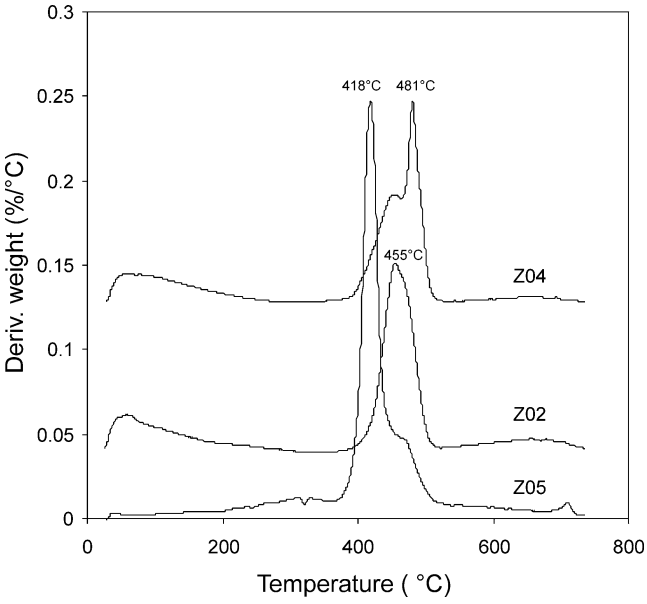

Fig. 5. DTG curves of as-synthesized MFI prepared under different conditions.

ditions. It is worth noting that the peaks in DTG curves correspond to the evolution temperature of template TPA^+ occluded in the channels of MFI and different peak temperatures correspond to different energetic sites in the channels of MFI from which TPA^+ is removed by thermal decomposition or desorption from MFI.

Fig. 5 clearly shows three types of DTG peaks located at 418, 455, and 481 °C, with the peak magnitude following this order: 418 > 455 > 481 °C. The peak at 418 °C, which occurs only for Z05, is a very strong peak in DTG profiles; this peak is suggested to be attributed to the unique energetic sites formed by Co incorporated into the MFI framework because the loading of Co in Z05 is as high as 4.21 wt%. It can be seen from Table 1 that the Na/Co ratio is only 0.14, showing that most cations required to balance the electrical neutrality of the MFI framework in Z05 are contributed by TPA^+, instead of Na^+.

The magnitude of the peak at 455 °C, which occurs for all samples, follows this order: Z02 [strong] ≫ Z04 [weak] > Z05 [shoulder]. This order is in good agreement with the order of CED of Co ions in the corresponding MFI, indicating that this peak is related to the cation-exchange sites in MFI. However, the DTG curves cannot confirm whether these energetic sites correspond to α-type Co^{2+} sites, β-type Co^{2+} sites, or both. The presence of the shoulder peak at 455 °C in Z05 accounts for the fact that few Co ions occupy cation positions and most of the Co species have been incorporated into the MFI framework. Since the peak at 455 °C is the only peak observed in Z02, this shows that Z02, which was synthesized at pH 13.5, possesses the largest amount of this kind of cation exchange sites. Although it is generally accepted that TPA^+ is a structurally directing agent during the synthesis of zeolite, the thermal removal of TPA^+ in Z02 is probably attributed to those TPA^+ cations that did not take part in the framework formation of MFI and these TPA^+ cations are competing with Na^+ to occupy the cation exchange sites. Therefore, the observation of only one peak temperature at 455 °C does not mean that there is only one kind of cation exchange site in Z02. However, since the peak magnitude at 455 °C is related to the CED of Co ions in MFI, this result suggests that most of the Co ions in Z02 have been exchanged at the cation sites corresponding to this DTG peak.

The DTG peak at 481 °C, which is located at the highest temperature and observed only for Z04, is attributed to those TPA^+ located at high energetic sites in MFI and hence corresponds to another cation-exchange site in MFI. However the cation-exchange process at this kind of site is hard to occur at ambient temperature, resulting in a much lower degree of Co ions exchanged in Z04 than in Z02. At this juncture, it is worth noting that DTG results not only confirm the presence of two different exchange Co ions, as reported in the literature [45–47], but also show the presence of a Co-incorporated site. In other words, we have shown that DTG can be used as a new method to characterize the presence of incorporated and exchangeable cation sites.

Our DTG results also indicate that the number of exchangeable cation positions in MFI depends on the pH of hydrothermal synthesis. The integrated intensity [% min/ °C] of all DTG peaks, which correspond to the total cation exchange capacity for all samples, is 0.84 for Z05, 0.58 for Z02, and 0.56 for Z04. The integrated intensity [% min/ °C] of DTG peaks in Z05 (0.84) is 45% higher that in Z02 (0.58), showing that divalent Co^{2+} ions incorporated into the framework of MFI need more TPA ions than trivalent Al^{3+}. In addition, the result of integrated intensity [% min/ °C] for DTG peaks shows that the total cation exchange capacity in Z04 is slightly lower than that in Z02 because the total integrated intensity of all DTG peaks in Z04 is 0.56, slightly lower than 0.58 of the peak at 455 °C in Z02. This DTG result is further confirmed by ICP chemical analysis which shows that the ratio of Si/Al in Z02 is lower than that in Z04 as well as by the fact that the lower the ratio of Si/Al in MFI, the higher the cation-exchange capacity.

3.3. TPR by hydrogen and XPS

Fig. 6 shows the TPR profiles of different cobalt-containing MFI. For reference, a TPR profile of 3.5 wt% of cobalt supported on γ-Al_2O_3 is also shown in Fig. 6. Two distinct reduction peaks at 512 and 598 °C are observed for Co/γ-Al_2O_3; these two peaks correspond to the reduction of Co_3O_4 to CoO and CoO to Co metal, respectively. Cobalt oxides on the surface of γ-Al_2O_3 are highly dispersed because the reduction temperatures for bulk Co_3O_4 to CoO and CoO to Co metal are 320 and 430 °C, respectively [56], which are much lower than those observed on Co/γ-Al_2O_3. A strong peak at 690 °C and a very weak peak at 290 °C are observed in Z05. Since this strong peak is 100 °C higher than

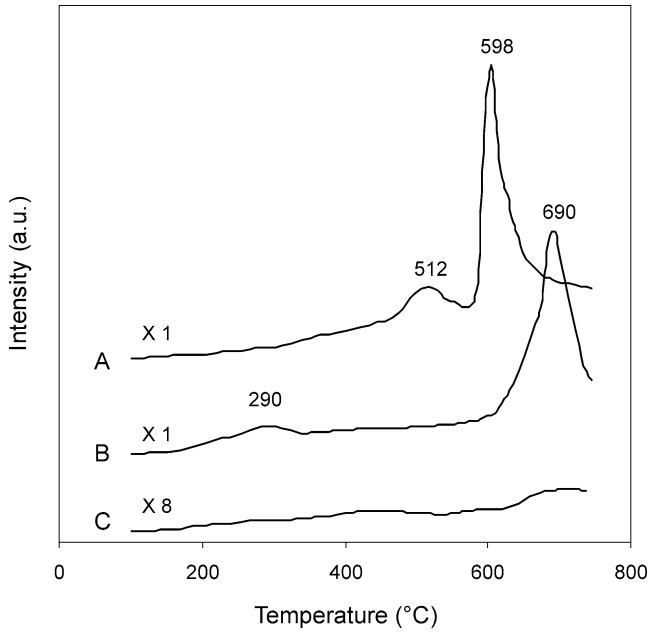

Fig. 6. Comparison of TPR profiles of different Co-containing samples: (A) Co_3O_4/γ-Al_2O_3, (B) Z05, and (C) Co-Z02.

that observed on Co/γ-Al_2O_3, it may be attributed to the reduction of incorporated cobalt in the MFI framework [56].

The TPR profile for Co-Z02 shows that no reduction peaks are observed up to 750 °C even with a TCD detector 8 times more sensitive than that used for Z05. This is not surprising as some researchers had similarly pointed out that cobalt species were nonreducible for Co-exchanged MFI [57–60]. EXAFS and XANES results indicated that the exchanged Co^{2+} has a distinct interaction with T atoms and it is the highly active site for NO reduction [44]. However, other researchers had observed a distinct reduction peak at about 700 °C for Co-exchanged MFI prepared from the conventional ion-exchange method at 80 °C [15,16] or at room temperature [21,35,42]. We believe that the discrepancies shown in the literature for the reduction of Co-exchanged MFI are attributed mainly to the structural difference of synthesized MFI materials. Since the exchangeable Co ions play a role in balancing the electrical neutrality of the framework, the reduction of these exchangeable Co ions depends on the following reaction:

$$Co^{2+}\text{–MFI} + H_2 \rightarrow Co + 2H^+\text{–MFI}. \quad (1)$$

The above reaction is thermodynamically unfavorable [$\Delta G^0 = +54.03$ kJ/mol] unless the framework structure is collapsed and/or the dealumination occurs during reduction by hydrogen. Therefore, the TPR peak for Co-exchanged MFI probably comes from the reduction of $Co[OH]^+$ [15,16] because the following reaction

$$Co[OH]^+\text{–MFI} + H_2 \rightarrow Co + H_2O + H^+\text{–MFI} \quad (2)$$

is thermodynamically more favorable than reaction (1). If $Co[OH]^+$ ions are present in MFI, the following reaction (3) can occur during calcination:

$$Co[OH]^+\text{–MFI} + Co[OH]^+\text{–MFI} \rightarrow Co^{2+}\text{–MFI} + CoO + H_2O. \quad (3)$$

Since the product CoO can be easily reduced by H_2, there should exist a weak TPR peak at 260 °C instead of the high-temperature peak at > 700 °C as reported in the literature [21]. However, Haack et al. [58] found that only a small fraction [< 5%] of cobalt oxide, which was present on the exterior surface of MFI crystallites, was reduced by H_2 to Co for Co-exchanged MFI, showing that a large amount of nonreducible Co^{2+}, not the $Co[OH]^+$, can exist in the interior of MFI crystallites.

XPS was also used in this study to characterize the chemical state of Co exchanged or incorporated in MFI. As shown in Fig. 7, for Co-exchanged MFI, the core level binding energy of $Co_{2p3/2}$ is at 781.7 eV, which is consistent with that reported elsewhere for a typical Co ion [58–61]. The split of the spin-orbital $2p_{3/2}$ and $2p_{1/2}$ peaks is at 15.6 eV, which is in agreement with that reported by Haack et al. [58] for Co^{2+}-exchanged MFI. In addition to these two spin-orbital peaks, two satellites for $2p_{3/2}$ and $2p_{1/2}$ are also observed, respectively, at 786.9 and 802.5 eV, indicating that the oxidation state of Co ions in Co-exchanged MFI is +2 [47]. Compared with the TPR profile for Co-Z02, which shows that the exchanged Co species in MFI are nonreducible, XPS spectra confirm that the nonreducible cobalt species are Co^{2+} ions at the exchangeable sites of MFI materials in this study.

The binding energies of $Co_{2p3/2}$ and $Co_{2p1/2}$ in Z05 are at 781.1 and 797.1 eV, respectively. Two satellites corresponding to the two spin-orbital peaks are located at 786.9 and 802.9 eV, respectively, showing that cobalt species in Z05 are +2. The split of the spin-orbital $2p_{3/2}$ and $2p_{1/2}$ peaks

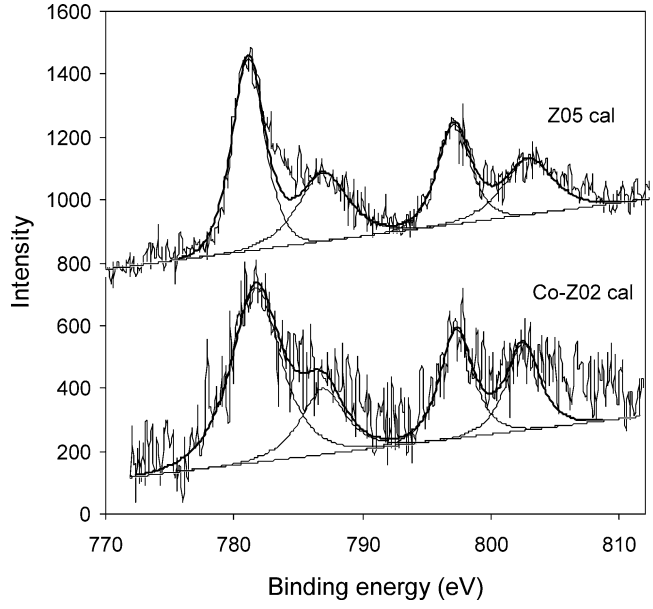

Fig. 7. XPS patterns of Co_{2p} on Co-incorporated and Co-exchanged MFI catalysts.

is 16.0 eV, consistent with that of CoO [62]. This demonstrates that the cobalt species in Z05 are present in the form of divalent ions covalently bonded to oxygen in MFI. The combined XRD, FTIR, and XPS results show that the cobalt species in Z05 are incorporated into the Si–O framework lattice of MFI by coordinating with oxygen. However, it should be noted that the binding energy of $Co_{2p3/2}$ as high as 782.7 eV has been reported for cobalt occupying MFI framework sites [63], where cobalt of high binding energy has been attributed to cobalt in a highly oxidized environment resulting from an interaction between the cobalt and the zeolite. In this work a weak TPR peak observed at 290 °C shows that most of the cobalt species in Z05 have been incorporated into the framework of MFI. Therefore, the binding energy of $Co_{2p3/2}$ for Co covalently coordinated with oxygen should be lower than that for Co^{2+} ionically coordinated at the exchangeable position, as only Co ions having pure ionic bonding, for example, those coordinated with F^-, have binding energy of $Co_{2p3/2}$ as high as 783.0 eV [61].

3.4. NO reduction activity

Fig. 8 shows the conversions of NO reduction and C_3H_8 oxidation over different cobalt-containing MFI catalysts. For all catalysts, the NO conversion displays a volcano-shape profile as the reaction temperature increases. The maximum NO conversion decreases in the following order: Co-Z02 > Co-Z04 > Z05. At the maximum conversion temperature of 450 °C, their NO conversions in the presence of 15 vol% of O_2 were 62.8, 29.3, and 11.8%, respectively. For Co-exchanged catalysts, a high level of exchange degree gives high conversion as the conversion of NO over Co-Z02 is much higher than that of Co-Z04 catalysts which have a lower ion-exchange degree. Co-incorporated MFI shows the lowest activity for NO SCR by propane as compared to Co-exchanged MFI, although the amount of cobalt in Z05 is as high as 4.21 wt%. In addition, the NO conversion profile over ion-exchanged catalysts increases with the increase of O_2 in the feed. For Co-Z04, the increase of O_2 concentration in the feed decreases the temperature required for maximum NO conversion. For Co-Z02, the maximum conversion temperature remains unchanged with increasing O_2 concentration in the feed.

It is seen from Fig. 8B that the increase of O_2 concentration enhances the oxidation of C_3H_8. The temperature required for 90% oxidation of C_3H_8 [T_{90}] decreases by about 50 °C with the increase of O_2 concentration from 5 to 15% over two Co-exchanged MFI catalysts. Furthermore, a higher loading of Co ions also enhances the oxidation: the T_{90} of C_3H_8 over Co-Z02 is 100 °C lower than that over Co-Z04 at different oxygen concentrations in the feed. For example, T_{90} of C_3H_8 with 15% of O_2 is 400 °C for Co-Z02 and 500 °C for Co-Z04 under the same reaction conditions. In other words, more C_3H_8 molecules can be activated over Co-Z02 than over Co-Z04 due to the higher content of Co^{2+} in Co-Z02 than in Co-Z04. The exchanged Co ions are more

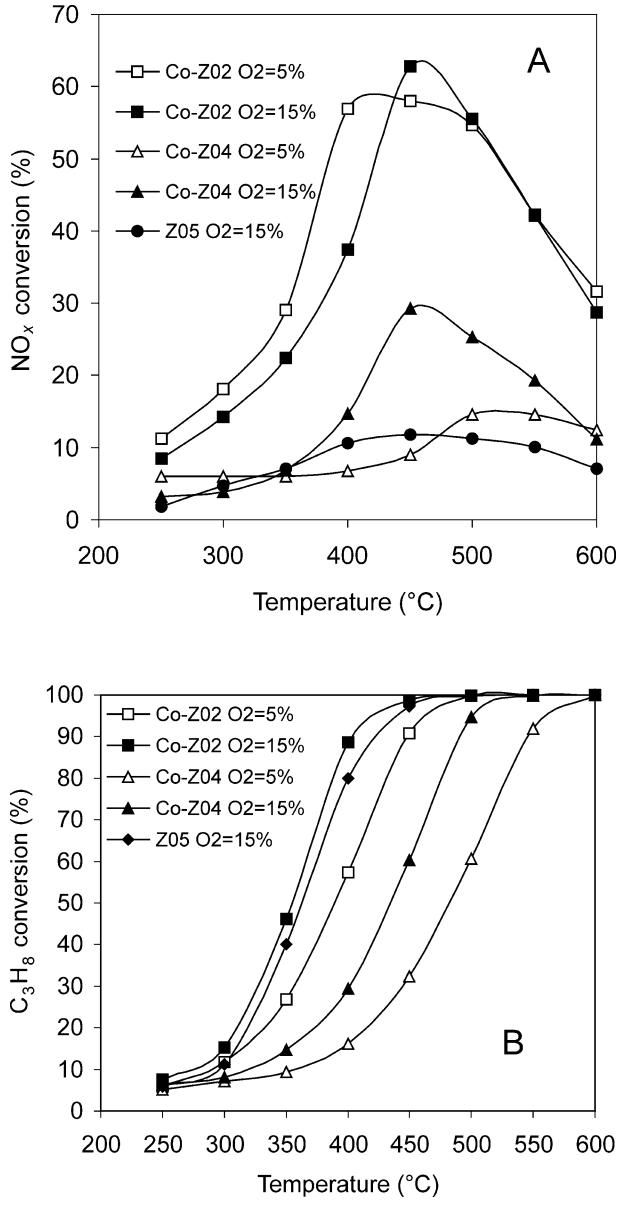

Fig. 8. Conversions of NO reduction and C_3H_8 oxidation over different cobalt-containing MFI under different O_2 concentrations (reaction conditions: 1000 ppm of NO, 1000 ppm of C_3H_8, space velocity = 15,000 h^{-1}).

active than incorporated Co species for oxidation of C_3H_8 as well as for the reduction of NO. The conversion of C_3H_8 in the presence of 15% of O_2 over Z05 is slightly lower than that over Co-Z02.

3.5. Comparison of TOF over different Co-exchanged MFI

The DTG results suggest that there are two types of cationic positions in our Co-exchanged MFI catalysts. To evaluate the activity of the Co ions exchanged into these different cationic sites for C_3H_8–SCR of NO, it is necessary to compare the TOF for NO reduction over these catalysts in order to find out the influence of different Co ions on NO conversion. It is worth noting that, for the NO–C_3H_8–O_2

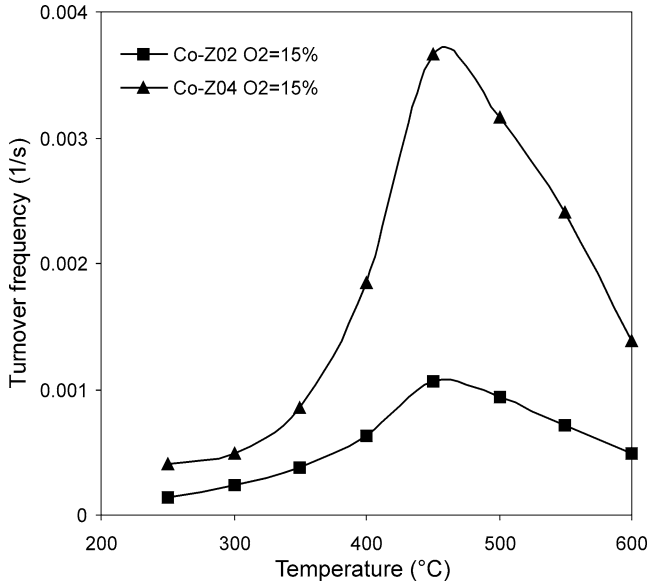

Fig. 9. Turnover frequency of NO in the presence 15% O_2 as a function of reaction temperature over Co-Z02 and Co-Z04 (the reaction conditions are the same as those in Fig. 8).

reaction system, the apparent reaction rate of NO reduction has been reported not to depend on the MFI-zeolite crystal size, showing that the reaction is not controlled by intracrystalline diffusion [64–66], although the pore size of MFI [$\sim$5.5 Å] has the same order of magnitude as the kinetic diameter of C_3H_8. However, the Co/Al ratio in MFI should still be kept to a low level in order to ensure that the reduction of NO is carried out under a kinetic-controlled region. The Co/Al ratio below 0.20 in our Co-exchanged MFI (see Table 1) is believed to satisfy this condition since the overall catalyst activity for C_3H_8–SCR of NO is found to increase linearly with the cobalt content in the range below Co/Al = 0.5 [20]. The TOF of NO reduction over these two types of Co^{2+}-exchanged MFI has been calculated from the results in Fig. 8, and these results of TOF vs reaction temperature are shown in Fig. 9. The volcano shape of TOF profiles, which is observable under increasing reaction temperature, is attributed to the competitive reaction of C_3H_8 with NO and O_2. In contrast to the NO conversion vs different Co ion levels, the TOF over Co-Z04 having a Co/Al ratio of 0.04 is much higher than that over Co-Z02 having a Co/Al ratio of 0.18. It can also be seen that the difference in TOF between Co-Z04 and Co-Z02 is a function of temperature. Below 350 °C, the difference in TOF remains constant with the increase of temperature. However, between 350 and 450 °C, the difference increases sharply with the increase of temperature. At 450 °C, the TOF corresponding to the maximum conversion of NO over Co-Z04 is 36.6×10^{-4} s^{-1}, which is 3.4 times higher than Co-Z02, although the total NO conversion over the latter is 2.14 times higher than the former. With a further increase of reaction temperature, the difference in TOF then decreases. The difference in TOF between Co-Z04 and Co-Z02 shows that there exist different types of exchangeable Co ions having different catalytic activities in MFI.

It is generally accepted that the temperature required for the maximum conversion of NO over Co-exchanged MFI is around 450 °C [3,15,16,28]. The temperature required for the maximum conversion of NO over Co-Z04 having low Co/Al ratio shifts to 500 °C when the O_2 concentration in the feed decreases from 15 to 5%, showing that the increase of O_2 in the feed facilitates the reduction of NO [3]. Actually the presence of O_2 mainly favors the activation of hydrocarbon by Co ions as Fig. 8B clearly indicates that the oxidation of C_3H_8 molecules depends strongly on the reaction temperature and the amount of Co^{2+} ions exchanged into MFI catalyst. For C_3H_8–SCR of NO in the presence of O_2, the oxidation of C_3H_8 can occur simultaneously as shown in the following two reactions:

$$2NO + C_3H_8 + 4O_2 \rightarrow N_2 + 4H_2O + 3CO_2, \quad (4)$$

$$C_3H_8 + 5O_2 \rightarrow 4H_2O + 3CO_2. \quad (5)$$

The above two reactions are parallel and competitive. The total conversion amount of NO in reaction (4) is proportional to the exchanged Co^{2+} loading in MFI. From a kinetic point of view, both NO conversion and propane oxidation increase with temperature, no matter how much active cobalt species are present in the catalyst. The selectivity of C_3H_8 [S] for the reduction of NO can be described as $S = [0.5\alpha_{NO}/\alpha_{C_3H_8}] \times 100\%$, where α_{NO} and $\alpha_{C_3H_8}$ correspond to the conversion of NO and C_3H_8, respectively. With a further increase in temperature, reaction (5) gradually predominates because it is thermodynamically more favorable than reaction (4). When the rate of reaction (5) becomes faster with the increase of temperature, reaction (4) reaches a maximum and then decreases due to the fact that most of the propane has been consumed by reaction (5) with increasing temperature. Therefore, the selectivity of C_3H_8 for NO reduction decreases with the increase of reaction temperature. As shown in Fig. 10, in the presence of 5% O_2, the selectivity of C_3H_8 over Co-Z02 catalysts decreases gradually from 95 to 20% with the increase of reaction temperature from 250 to 600 °C. A similar performance trend is observed over the Co-Z04 sample. In the presence of 15% O_2 in the reaction system, the selectivity of C_3H_8 over Co-Z02 decreases quickly from 56 to 21% with increasing reaction temperature from 250 to 400 °C and the selectivity is lower than that in the presence of 5% O_2 as the competition of reaction (5) is facilitated at high concentrations of O_2. The selectivity of C_3H_8 increases to a peak at 450 °C, which is the most active reaction temperature for NO reduction with 15% of O_2 in the reaction system. Above that temperature the oxidation of C_3H_8 [reaction (5)] gradually dominates the overall reaction and selectivity of C_3H_8 decreases with the rise of temperature. It is interesting to note that over the Co-Z04 sample, in the presence of 15% of O_2, the selectivity of C_3H_8 is quite stable below 450 °C where C_3H_8 is not completely converted and the competition between reactions (4) and (5) is balanced with variation of reaction

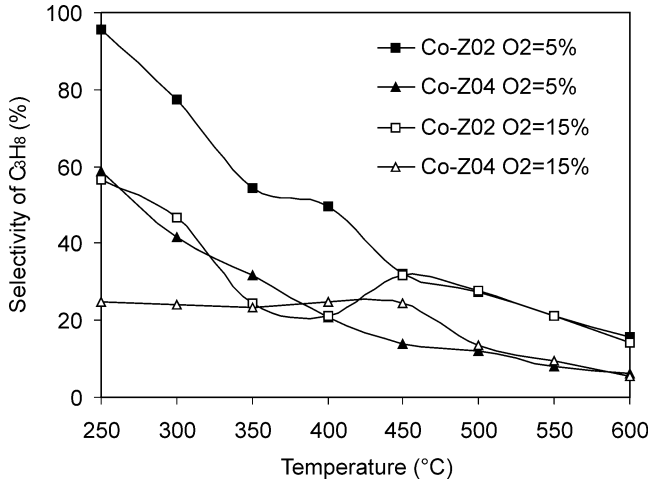

Fig. 10. Selectivity of C_3H_8 (derived from Fig. 8) for the reduction of NO as a function of temperature over Co^{2+}-exchanged MFI.

temperature. Only above this temperature, all C_3H_8 is completely oxidized in the overall reaction and the completion of reaction (4) is weakened, thus resulting in the decrease of the selectivity of C_3H_8 for SCR of NO.

The different Co^{2+}-exchange capacities in Z02 and Z04 are suggested to be attributed to the presence of different surface energetic sites for cation exchange in MFI. There exist at least two types of cation-exchange positions in different MFI. The Co ions located at high energetic sites have higher reduction activity for NO than those located at low energetic sites. These low and high energetic sites probably correspond to alpha- and beta-type Co ion sites as reported in the literature [45–47]. However, it should be noted here that the high-energy exchange sites observed in this study are hard to be exchanged with Co ions. DTG analysis is believed to be used successfully in this work to relate SCR of NO over Co/MFI to the location of cobalt species. As compared to C_3H_8–SCR of NO, three peaks in DTG profiles correspond well to three types of energetic sites in MFI. The Co species located in these sites show different SCR activities: the DTG peak at 418 °C corresponds to the inactive incorporated Co and the DTG peaks at 455 and 481 °C correspond to two different Co ions having different activities. By comparing DTG peaks with SCR of NO, Co-Z04 is found to contain two types of Co ions. The Co ions located at high energetic sites, which correspond to the DTG peak at 481 °C, have higher reduction activity than those located at low energetic sites, which correspond to the DTG peak at 455 °C. However, Co ions are hard to be exchanged into these high energetic or active sites unless special ion-exchange methods are used [15,16]. In addition to those reported in the literature [67] where different cationic sites have been reported to be controlled by the content of the framework Al in MFI, we have shown in this work that the formation of different cationic sites depends on the pH used in the hydrothermal synthesis of MFI.

4. Conclusions

Different Co species, those exchanged and incorporated in MFI, are synthesized under different pH and used for selective catalytic reduction of NO by propane in the presence of excess O_2. The incorporated cobalt in MFI is inactive for NO reduction by C_3H_8 in the presence of excess oxygen. For Co^{2+}-exchanged MFI, the exchange degree of Co^{2+} in MFI depends greatly on the alkalinity of the synthesis system. MFI synthesized at high alkalinity [pH 13.5] gives a higher level of exchanged Co ions than that synthesized at low alkalinity [pH 12]. The sample having a high ion-exchange level of Co^{2+} shows higher NO conversion than that having a low ion-exchange level. However, Co^{2+} ions in MFI having a low level of ion-exchange capacity have a higher TOF than those having high-level exchange, suggesting that at least two types of Co ions having different activity for C_3H_8–SCR of NO exist in Co-exchanged MFI. Differential thermogravimetric analysis (DTG) is used to relate the activity of Co species in MFI with the activity of C_3H_8–SCR of NO. A comparison of the reduction activity of NO with those peaks for the thermal decomposition or disassociation of TPA suggests that the exchangeable cationic positions and incorporated sites correspond to different energetic sites in MFI. Those Co^{2+} ions located at high energetic positions in MFI seem to have high specific catalytic activities for NO reduction.

Acknowledgments

This research work has been generously supported by the National University of Singapore (R-279-000-093-112) and the National Science and Technology Board of Singapore (R-279-000-093-303).

References

[1] M. Iwamoto, H. Yahiro, Y. Yu-u, S. Shundo, N. Mizuno, Shokubai 32 (1990) 430.
[2] W. Held, A. König, T. Richter, L. Puppe, SAE Trans., Sect. 4 No. 900 496 (1990) 209.
[3] Y. Li, J.N. Armor, Appl. Catal. B 1 (1992) L31.
[4] Y. Li, J.N. Armor, Appl. Catal. B 2 (1993) 239.
[5] Y. Li, J.N. Armor, Appl. Catal. B 4 (1994) L11.
[6] Y. Li, P.J. Battavio, J.N. Armor, J. Catal. 142 (1993) 561.
[7] H. Hamada, Y. Kintaichi, M. Sasaki, T. Ito, Appl. Catal. 75 (1991) L1.
[8] T. Inui, S. Iwamoto, S. Shimizu, in: R. von Ballmoons, J.B. Higgins, M.M.J. Treacy (Eds.), Proceedings of the 9th International Zeolite Conference, Vol. 2, Montreal, Butterworth–Heinemann, Boston, 1993, p. 405.
[9] S. Iwamoto, S. Kon, S. Yoshida, T. Inui, Stud. Surf. Sci. Catal. 105 (1997) 1587.
[10] T. Inui, S. Iwamoto, S. Kojo, S. Shimizu, T. Hirabayashi, Catal. Today 22 (1994) 41.
[11] K. Kagawa, Y. Ichikawa, S. Iwamoto, T. Inui, Catal. Lett. 52 (1998) 145.
[12] B.J. Adelman, T. Beutel, G.-D. Lei, W.M.H. Sachtler, J. Catal. 158 (1996) 327.

[13] J.-Y. Yan, H.H. Kung, W.M.H. Sachtler, M.C. Kung, J. Catal. 175 (1998) 294.
[14] X. Wang, H.-Y. Chen, W.M.H. Sachtler, J. Catal. 197 (2001) 281.
[15] X. Wang, H.-Y. Chen, W.M.H. Sachtler, Appl. Catal. B 26 (2000) L227.
[16] X. Wang, H.-Y. Chen, W.M.H. Sachtler, Appl. Catal. B 29 (2001) 47.
[17] T. Tabata, H. Ohtsuka, L.M.F. Sabatino, G. Bellussi, Micropor. Mesopor. Mater. 21 (1998) 517.
[18] T. Tabata, H. Ohtsuka, Catal. Lett. 48 (1997) 203.
[19] T. Tabata, M. Kokitsu, H. Ohtsuka, O. Okada, L.M.F. Sabatino, G. Bellussi, Catal. Today 27 (1996) 91.
[20] A.Y. Stakheev, C.W. Lee, S.J. Park, P.J. Chong, Appl. Catal. B 9 (1996) 65.
[21] A.Y. Stakheev, C.W. Lee, S.J. Park, P.J. Chong, Catal. Lett. 38 (1996) 271.
[22] C.W. Lee, P.J. Chong, Y.C. Lee, C.S. Chin, L. Kevan, Catal. Lett. 48 (1997) 129.
[23] D.B. Lukyanov, G.A. Sill, J.L. d'Itri, W.K. Hall, J. Catal. 153 (1995) 265.
[24] D.B. Lukyanov, E.A. Lombardo, G.A. Sill, J.L. d'Itri, W.K. Hall, J. Catal. 163 (1996) 447.
[25] A.J. Desai, V.I. Kovalchuk, E.A. Lombardo, J.L. d'Itri, J. Catal. 184 (1999) 396.
[26] A.T. Bell, Catal. Today 38 (1997) 151.
[27] J.T. Miller, E. Glusker, R. Peddi, T. Zheng, J.R. Regalbuto, Catal. Lett. 51 (1998) 15.
[28] F. Witzel, W.K. Hall, J. Catal. 149 (1994) 229.
[29] M.C. Campa, S. De Rossi, G. Ferraris, V. Indovina, Appl. Catal. B 8 (1996) 315.
[30] D. Kaucky, A. Vondrova, J. Dedecek, B. Wichterlova, J. Catal. 194 (2000) 318.
[31] S.K. Park, Y.-K. Park, S.-E. Park, L. Kevan, Phys. Chem. Chem. Phys. 2 (2000) 5500.
[32] M.D. Amiridis, T. Zhang, R.J. Farrauto, Appl. Catal. B 10 (1996) 203.
[33] A.D. Cowan, R. Dumpelmann, N.W. Cant, J. Catal. 151 (1995) 356.
[34] Y.-F. Chang, J.G. McCarty, J. Catal. 178 (1998) 408.
[35] L. Gutierrez, A. Boix, J.O. Petunchi, J. Catal. 179 (1998) 179.
[36] V.I. Parvulescu, P. Grange, B. Delmon, Catal. Today 46 (1998) 233.
[37] A.P. Walker, Catal. Today 26 (1995) 107.
[38] B. Wen, W.M.H. Sachtler, Catal. Lett. 86 (2003) 39.
[39] S.C. Shen, S. Kawi, Catal. Today 68 (2001) 245.
[40] S.C. Shen, S. Kawi, J. Catal. 213 (2003) 241.
[41] Y. Li, J.N. Armor, Appl. Catal. B 1 (1992) L21.
[42] R.S. da Cruz, A.J.S. Mascarenhas, H.M.S. Andrade, Appl. Catal. B 18 (1998) 223.
[43] Y. Li, J.N. Armor, J. Catal. 150 (1994) 376.
[44] V. Schwartz, R. Prins, X. Wang, W.M.H. Sachtler, J. Phys. Chem. B 106 (2002) 7210.
[45] E.-M. El-Malki, D. Werst, P.E. Doan, W.M.H. Sachtler, J. Phys. Chem. B 104 (2000) 5924.
[46] J. Dedecek, D. Kaucky, B. Wichterlova, Micropor. Mesopor. Mater. 35–36 (2000) 483.
[47] T. Sun, M.L. Trudeau, J.Y. Ying, J. Phys. Chem. 100 (1996) 13662.
[48] J. Dedecek, D. Kaucky, B. Wichterlova, Top. Catal. 18 (2002) 283.
[49] S. Sato, Y. Yu, H. Yahiro, N. Mizuno, M. Iwamoto, Appl. Catal. A 70 (1997) 129.
[50] R.A. Kensington, G.R. Landolt, US patent 3,702,886, 1972.
[51] S.J. Jong, S. Cheng, Appl. Catal. A 126 (1995) 51.
[52] H.Y. Zhu, N. Maes, A. Molinard, E.F. Vansant, Micropor. Mater. 3 (1994) 235.
[53] E.M. Flanigen, in: J.A. Rabo (Ed.), Zeolite Chemistry and Catalysis, Adv. Chem. Series, Vol. 171, Am. Chem. Society, Washington, DC, 1976, Chapter 2.
[54] G. Coudurier, C. Naccache, J.C. Vedrine, J. Chem. Soc., Chem. Commun. (1982) 1413.
[55] J.C. Jansen, F.J. van der Gaag, H. van Bekkum, Zeolites 4 (1984) 369.
[56] S.J. Jong, S. Cheng, Appl. Catal. A 126 (1995) 51.
[57] J.M. Stencel, V.U.S. Rao, J.R. Diehl, K.H. Rhee, A.G. Dhere, R.J. DeAngelis, J. Catal. 84 (1983) 109.
[58] L.P. Haack, C.P. Hubbard, M. Shelef, in: U.S. Ozkan, S.K. Agarwal, G. Marcelin (Eds.), Reduction of Nitrogen Oxide Emissions, in: ACS Symposium Series, Vol. 587, Am. Chem. Society, Washington, DC, 1995, p. 166.
[59] Q. Wei, C. Ying, Gaodeng Xuexiao Huaxue Xuebao 12 (1991) 80.
[60] V.U.S. Rao, Phys. Scripta T 4 (1983) 71.
[61] J.F. Moulder, W.F. Stickle, P.E. Sobol, K.D. Bomben, in: J. Chastain (Ed.), Handbook of X-Ray Photoelectron Spectroscopy: A Reference Book of Standard Spectra for Identification and Interpretation of XPS Data, Perkin–Elmer, Eden Prairie, MN, 1992.
[62] T.J. Chung, C.R. Brundle, D.W. Rice, Surf. Sci. 59 (1976) 413.
[63] J.A. Rossin, C. Saldarriaga, M.E. Davis, Zeolites 7 (1987) 295.
[64] A. Shichi, A. Satsuma, S. Komai, T. Hattori, J. Chem. Eng. JP 34 (2001) 102.
[65] A. Shichi, K. Katagi, A. Satsuma, T. Hattori, Appl. Catal. B 24 (2000) 97.
[66] T. Masuda, Y. Okubo, S.R. Mukai, M. Kawase, K. Hashimoto, A. Shichi, A. Satsuma, T. Hattori, Y. Kiyozumi, Chem. Eng. Sci. 56 (2001) 889.
[67] J. Dedecek, B. Wichterlova, J. Phys. Chem. 98 (1994) 5721.